

Tri-critical point and suppression of the Shastry-Sutherland phase in $\text{Ce}_2\text{Pd}_2\text{Sn}$ by Ni doping

J.G. Sereni¹, G. Schmerber², M. Gómez Berisso¹, B. Chevalier³ and J.P. Kappler²

¹ *Div. Bajas Temperaturas, CAB-CNEA and Conicet, 8400 S. C. de Bariloche, Argentina*

² *IPCMS, UMR 7504 CNRS-ULP, 23 rue de Loess, B.P. 43 Strasbourg Cedex 2, France*

³ *CNRS, Université de Bordeaux, ICMCB, 87 av. Dr. Schweitzer, 33608 Pessac Cedex, France*

(Dated: October 29, 2018)

Structural, magnetization and heat capacity measurements were performed on $\text{Ce}_2(\text{Pd}_{1-x}\text{Ni}_x)_2\text{Sn}$ ($0 \leq x \leq 0.25$) alloys, covering the full range of the Mo_2FeB_2 structure stability. In this system, the two transitions observed in $\text{Ce}_2\text{Pd}_2\text{Sn}$ (at $T_N = 4.8\text{K}$ and $T_C = 2.1\text{K}$ respectively) converge into a tri-critical point at $T_{cr} \approx 3.4\text{K}$ for $x \approx 0.3$, where the intermediate antiferromagnetic AF phase is suppressed. The $T_N(x)$ phase boundary decrease is due to an incipient Kondo screening of the Ce-4f moments and local atomic disorder in the alloy. Both mechanisms affect the formation of Ce-magnetic dimers on which the Shastry-Sutherland lattice (SSL) builds up. On the contrary, the $T_C(x)$ transition to the ferromagnetic ground state increases as a consequence of the weakening of the AF-SSL phase. Applied magnetic field also suppresses the AF phase like in the stoichiometric compound.

Keywords: Cerium compounds, Critical Points, Magnetic Phase Diagrams, Magnetic transitions

* E-mail-address of corresponding author: jsereni@cab.cnea.gov.ar

I. INTRODUCTION

Crystalline structures with local symmetries which favor magnetic frustration attract special interest because they provide the scenario for novel phases formation. In many cases, magnetic frustration or exotic phases occur in competition with classical long range order ground states GS. Thus, the search of exotic phases is addressed to the vicinity of magnetic transitions, since the 'roughness' of the free energy may develop new relative minima as a function of a non trivial order parameter [1]. Those minima compete in energy for the formation of novel phases, which may become unstable under small variation of control parameters like magnetic field, alloying or pressure.

Beside the mentioned frustrated states, alternative phases may occur under peculiar geometrical conditions. Among them, the so called Shastry-Sutherland lattice (SSL) [2, 3] builds up from mutually orthogonal magnetic dimers which impose further topological and magnetic constrains. These conditions are realized in some members of the $\text{R}_2\text{T}_2\text{X}$ family of compounds (with R = Rare Earths or Actinides, T = Transitions Metals and X = 'p' type metalloids), which crystallize in tetragonal Mo_2FeB_2 structure [4]. In that structure, each 'R' layer forms a mosaic of magnetic atoms coordinated as isosceles triangles between nearest- and next nearest neighbors centered on the z -axis of the T element. The shortest side of those triangles, where R-R magnetic dimers form, is shared by two consecutive triangles like in the shortest diagonal of a rhombohedron. The resulting simple square-lattice of mutually orthogonal rhombohedron mimicks a sort of 'pinwheel' centered on the z -axis of the X element [5], whereas the net of dimers form a simple two dimensional (2D) square lattice.

Recently, SSL phases were found in a number of $\text{R}_2\text{T}_2\text{X}$

compounds [5, 6] and the involved magnetic interactions theoretically discussed [7]. In $\text{Ce}_2\text{Pd}_2\text{X}$ compounds, where Ce-Ce dimers form due to a nearest neighbor ferromagnetic FM interaction, the SSL phase shows up within a limited range of temperature (c.f. between $T_N = 4.8\text{K}$ and $T_C = 2.1\text{K}$ in $\text{Ce}_2\text{Pd}_2\text{Sn}$ [5]). Below T_C , a FM-GS takes over undergoing a first order transition due to the discontinuity in the order parameter. Further studies performed under magnetic field on the mentioned compound [8] showed that the intermediate phase is suppressed applying a magnetic field $B_{cr} \approx 0.12\text{T}$ at $T_{cr} \approx 3.2\text{K}$. The fact that the SSL phase is suppressed by quite low magnetic field in $\text{Ce}_2\text{Pd}_2\text{Sn}$ remarks its instability respect to a 3D FM magnetic structure as GS.

In this work we have investigated Ni doped $\text{Ce}_2(\text{Pd}_{1-x}\text{Ni}_x)_2\text{Sn}$ alloys with the scope to compare the effect of structural pressure and magnetic field on the stability of the SSL phase. Since Pd and Ni are iso-electronic elements, but being Ni atoms about 25% smaller in volume than Pd ones, an effective structural pressure is expected to weak the Ce-4f magnetic moments. Similarly, applied magnetic field shall progressively suppress the SSL phase like in the stoichiometric compound.

In a former study performed on this system [9], no change of structure was reported under Ni doping. The unit cell volume was reported to follow a Vergard's law up to $x = 0.6$, with the paramagnetic Curie-Weiss temperature θ_P decreasing from 20 K at $x = 0$ to -40 K at $x = 0.5$. Electrical resistivity (ρ) was observed to be nearly temperature independent with a high value of ρ_0 and large difference upon cooling and heating, which was interpreted as due to cracks in the alloyed samples [9]. However, in a recent investigation, a change of structure was detected at $x = 0.35 \pm 0.05$ [10]. Thus, the large ρ_0 values and the abnormal $\rho(T)$ dependence can be explained as due to non single crystalline phases in the

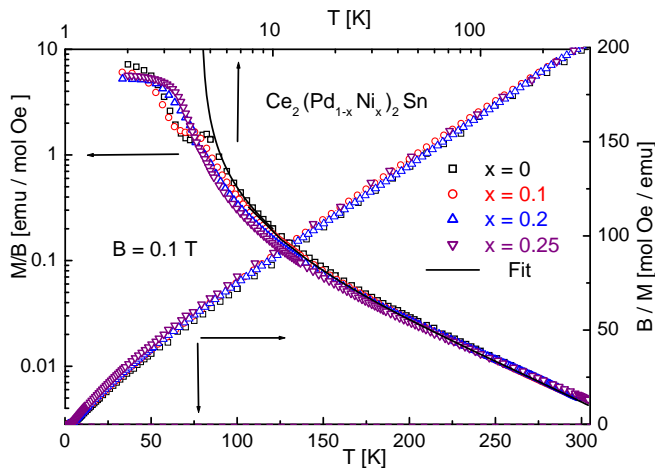


FIG. 1. (Color online) High temperature magnetic susceptibility in a Log-Log representation for different Ni concentrations (left and upper axes) and inverse susceptibility (right and lower axes).

concentration region where the system presents a coexistence of two crystalline structures.

II. EXPERIMENTAL DETAILS AND RESULTS

Details for sample preparation were described in a previous paper [5]. Structural characterization confirms the single phase composition of the samples in a tetragonal Mo_2FeB_2 -type structure for $x < 0.3$. Beyond a short range of coexistence of two phases, this system stabilizes in an orthorhombic W_2CoB_2 type structure for $x > 0.4$ [10]. The actual composition of the stoichiometric compound was determined to be $\text{Ce}_{2.005}\text{Pd}_{1.988}\text{Sn}_{0.997}$ after SEM/EDAX analysis. Lattice parameters slightly decrease with Ni concentration from $a = 7.765\text{\AA}$ and $c = 3.902\text{\AA}$ at $x = 0$, to $a = 7.7122\text{\AA}$ and $c = 3.8941\text{\AA}$ at $x = 0.25$. These variations drive a reduction of the unit cell volume of about $\approx 1.5\%$ between $x = 0$ and 0.25 . On the contrary, the 'c/a' ratio practically does not change, indicating that the local symmetry is not affected by doping.

DC-magnetization measurements were carried out using a standard SQUID magnetometer operating between 2 and 300 K, and as a function of field up to 5 T. Specific heat was measured using standard heat pulse technique in a semi-adiabatic He-3 calorimeter in the range between 0.5 and 20 K, at zero and applied magnetic field up to 4 T. The magnetic contribution to the the specific heat C_m was computed subtracting the phonon contribution extracted from the isotypic $\text{La}_2\text{Pd}_2\text{Sn}$ compound. Electrical resistivity was measured between 0.5 K and room temperature using a standard four probe technique with an LR700 bridge. However, sample cracking inhibits to extract valuable information from $\rho(T)$ data.

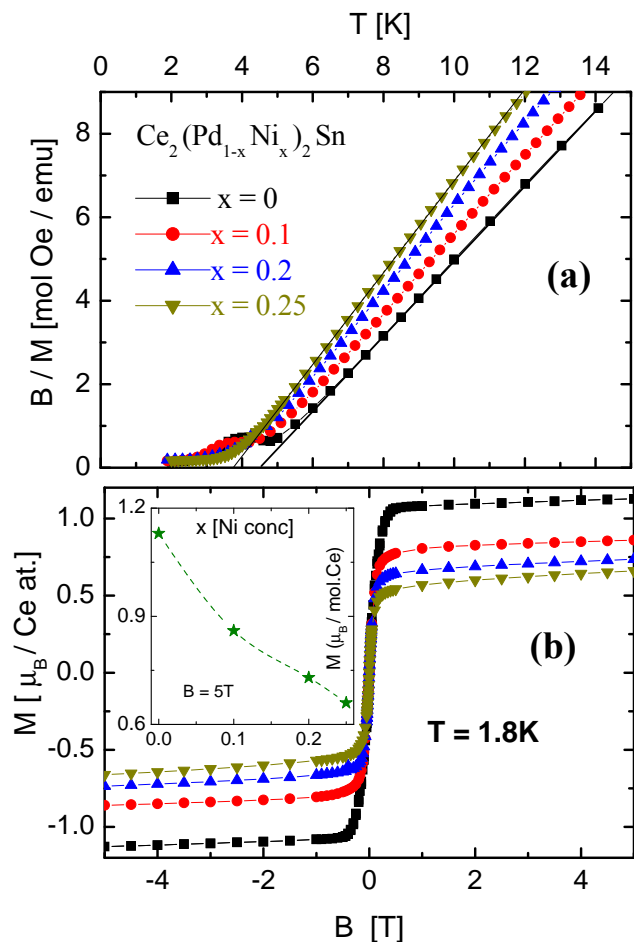


FIG. 2. (Color online) (a) Low temperature inverse magnetic susceptibility showing the variation of θ_p^{LT} , measured with $B = 0.1\text{ T}$. (b) Field magnetization within the FM phase, showing the decrease of the saturation moment with Ni concentration increase. Inset: magnetic moment at $B = 5\text{ T}$ within the $x \leq 0.25$ range.

A. Ni concentration dependent properties

As shown in Fig. 1, Ni doping does not affect significantly the magnetic susceptibility (χ) at high temperature. Fits of $\chi(T)$ do not show significant variation of crystal field effect (CEF) from the values observed in stoichiometric $\text{Ce}_2\text{Pd}_2\text{Sn}$ [5], with respective splitting at $\Delta_I = 65 \pm 5\text{ K}$ and $\Delta_{II} = 240 \pm 10\text{ K}$. From the inverse of $\chi(T)$, one extracts that the high temperature θ_p^{HT} slightly increases only for $x \geq 0.2$ from -16 K to -25 K . This indicates that only a minor hybridization increase occurs for the CEF excited levels within this range of Ni doping. Coincidentally, the high temperature Ce magnetic moment practically does not change from its Ce^{3+} value.

A different behavior is observed at low temperature, where $\theta_p^{LT} > 0$. Its value decreases from 4.5 K (at $x = 0$)

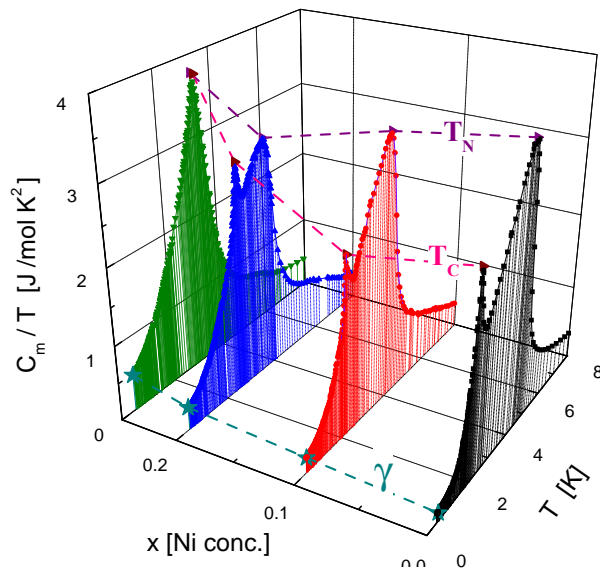


FIG. 3. (Color online) Evolution of the magnetic specific heat divided T for $\text{Ce}_2(\text{Pd}_{1-x}\text{Ni}_x)_2\text{Sn}$ showing the convergent variation of both transitions AF- T_N and FM- T_C converging at $x_{cr} \geq 0.25$. Dashed line labeled γ represents a rising heavy fermion contribution.

to 3.7 K (at $x = 0.25$), as shown in Fig. 2a, indicating a moderate Ni doping effect on the doublet GS magnetism. This goes hand by hand with the magnetic saturation extracted from field dependent magnetization measurements (see Fig. 2b), performed at $T = 1.8$ K within the FM phase. Also the cusp of $M(T)$ at $T = T_N$ is reduced till it is overcome by the FM contribution (see Fig. 4a).

In the case of specific heat, Ni concentration affects quite significantly the $C_m(T)$ jumps of both transitions as shown in Fig. 3. While the temperature of the upper one decreases from $T_N(x = 0) = 4.8$ K to $T_N(x = 0.25) \approx 3.5$ K, the lower transition increases from $T_C(x = 0) = 2.1$ K up to $T_C(x = 0.25) \approx 3.3$ K (see inset in Fig. 4a). These opposite Ni dependencies drive the transitions to merge at a tri-critical point at $T_{cr} \approx 3.4$ K, just above the highest Ni concentration studied ($x = 0.25$).

$T_N(x)$ is a second order transition, whereas $T_C(x)$ is of first order. This character is recognized by an hysteretic $C_m(T)$ dependence measured around T_C and reflects the discontinuity in the magnetic order parameter at $T = T_C$. Both $C_m(T)$ maxima decrease with Ni doping, however as they merge into an unique maximum the $C_m(T)$ cusp clearly rises. Notice the sharpness of the cusp in sample $x = 0.25$ revealing its vicinity to the critical point.

B. Magnetic field effects

Doping and magnetic field effects coincide enhancing the FM character of the GS phase with the consequent $T_C(x, B)$ increase. On the contrary, while Ni doping over-

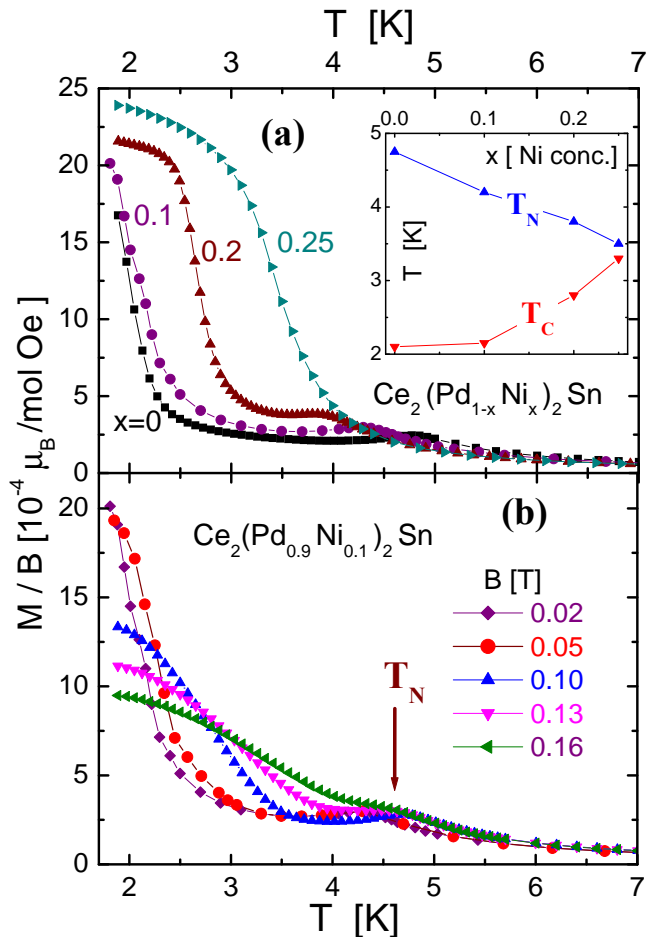


FIG. 4. (Color online) Comparison of the thermal dependence of magnetization around AF and FM transitions: (a) as a function of Ni doping (with $B = 0.02$ T). Inset: $T_N(x)$ and $T_C(x)$ dependencies. (b) Magnetic field effect on the $x = 0.1$ sample.

duces a decrease of $T_N(x)$ magnetic field practically does not affect the upper transition. The doping effect can be observed in Fig. 4a, which shows how the temperature of the spontaneous magnetization (related to T_C) increases, overlapping the $M(T_N)$ cusp as Ni content increases.

In the case of applied magnetic field, one can observe in Fig. 4b for sample $x = 0.1$ how the temperature of the $M(T_N)$ cusp remains practically unchanged. The same behavior was observed in the stoichiometric compound [8] and is confirmed in sample $x = 0.2$. In the case of sample $x = 0.25$, the T_N cusp is already overlapped by the FM signal at very low applied field. One have to remind that, apart from the $T_C(x)$ increase, the FM transition is smeared under applied magnetic field and therefore the high temperature tail of the FM magnetization overcomes the T_N cusp faster than the actual increase of $T_C(x)$.

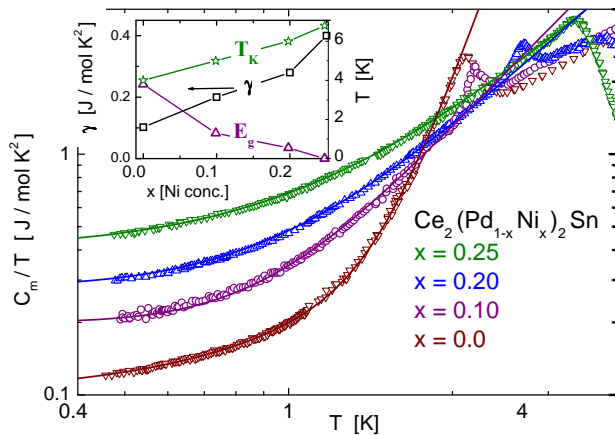


FIG. 5. (Color online) Analysis of the $C_m(T)/T$ dependence for $T < T_C$ in a Log-Log representation. Continuous curves are fits from which γ and magnon gaps E_g are extracted, see the text. Inset: Ni concentration dependence of $\gamma(x)$ (left axis), and $E_g(x)$ and Kondo temperature $T_K(x)$ (right axis).

III. DISCUSSION

A. Specific heat Gap

Relevant information related to the magnetic structure of this system can be extracted from the analysis of the thermal dependence of the specific heat within the ordered phase. Since the $x = 0$ sample have shown strong anisotropic effects, we have analyzed the magnetic contribution of the FM phase to $C_m(T)$ by fitting all curves with an unique function in order to evaluate the variation of the characteristic parameters as a function of Ni content. The simplest applicable function is $C_m/T = \gamma + AT^2 \exp(-E_g/T)$, where the γ term accounts for the degrees of freedom behaving as a Kondo liquid and E_g represents the energy (expressed in temperature) of the gap of anisotropy in the magnon spectrum. Respective fits are included in Fig. 5 using a double logarithmic scale, and computed values are collected in the inset. These results indicate that the specific heat behaves as that of systems whose gap of anisotropy decreases to zero when approaching the critical concentration. Coincidentally, the γ contribution increases with Ni content.

B. Entropy and Kondo Temperature

From the thermal variation of the magnetic contribution to the entropy (S_m), the effect of Ni doping on the Ce-4f magnetic moment can be traced. As it can be observed in Fig. 6, it is only for $x \geq 0.2$ that some incipient hybridization effect can be detected. To extract the Kondo temperature variation, we have applied the

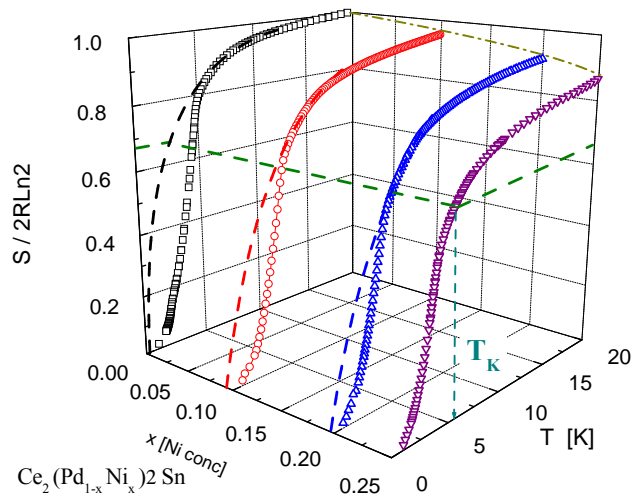


FIG. 6. (Color online) Thermal dependence of the entropy for the studied samples in a 3D representation. Dashed curves indicate the extrapolation of $S_m(T)$ from $T > T_N$ to $T < T_N$, and the straight lines the $S_m = 0.662Rln2$ value from which T_K is extracted.

current Desgranges-Schotte criterium [11] from which at $T = T_K$ the entropy reaches the value $S_m = 0.66Rln2$. Notice that in our case the comparison has to be done in $2Rln2$ units because there are two Ce atoms contained in a formula unit of this compound. Since this model was proposed for single impurities, the $S_m(T)$ curve has to be extrapolated from $T > T_N$ following the curvature within the non-interacting (paramagnetic) phase, which does not account for the condensation of degrees of freedom into the ordered state. Despite of the small error introduced by this extrapolation, the relevant information extracted is the low value of T_K ($T_K \approx 4$ K for $x = 0$) and its variation with concentration ($T_K \approx 7$ K for $x = 0.25$). The computed $T_K(x)$ values are included in the inset of Fig. 5. There is an apparent contradiction in this coincident increase of $T_K(x)$ and $\gamma(x)$ because they are expected to depend inversely to each other (i.e. $\gamma \propto T_K$). This behavior can be explained by the fact that T_K is an *intensive* parameter (i.e. a scale of energy) which increases with x , and γ is *pseudo-intensive* because it depends on the degrees of freedom involved in the Kondo liquid contribution. From this comparison we conclude that there is a gradual transference of degrees of freedom from the ordered phase to the Kondo liquid component.

C. Stability of the SSL phase versus doping

In order to investigate up to which extend Ni doping affects the stability of the SSL phase, we have studied the magnetic field effect in the alloyed samples follow-

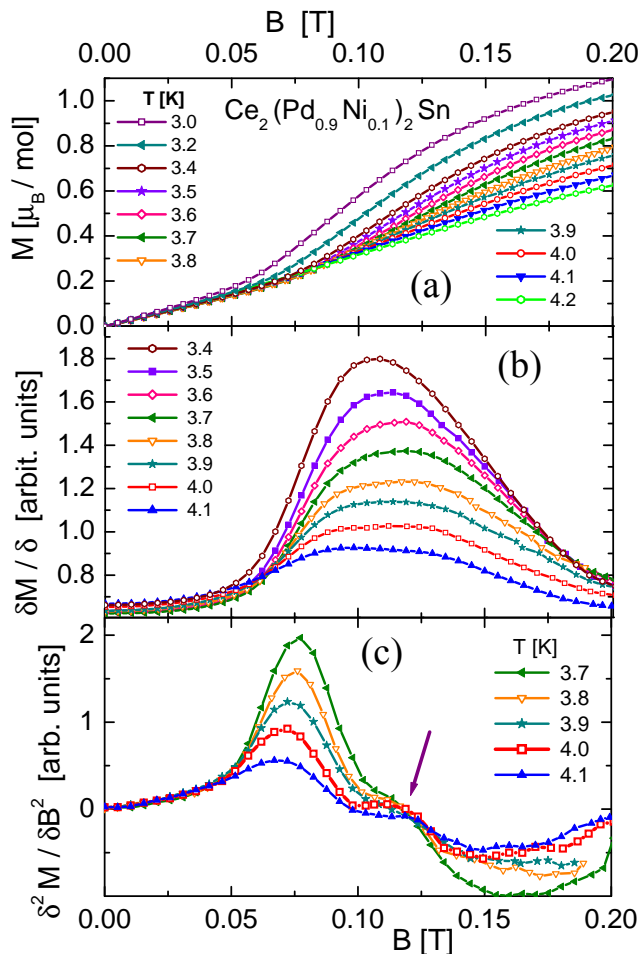


FIG. 7. (Color online) (a) Field dependence of magnetization of sample $x = 0.1$ between 3 and 4.2 K. (b) First derivative and (c) second derivative for the $3.7 \text{ leq} T \leq 4.1 \text{ K}$ range, with the arrow indicating the satellite anomaly.

ing the same procedure like in the stoichiometric compound ($x = 0$) [8]. Starting with the $x = 0.1$ sample, we have performed $M(B)$ measurements within the range of temperature where the features related to the SSL phase could be detected, see Fig. 7a. Above T_C , the $M(B)$ isotherms show a 'S' shape reflecting an AF character, which is rapidly polarized by magnetic field. There is however a crossing of magnetization curves around $B = 0.11 \text{ T}$ followed by a slight modulation which was taken as indication of a SSL formation in the stoichiometric compound [8]. Further information was extracted from the $\partial M / \partial B|_T$ derivative shown in Fig. 7b. An incipient shoulder can be appreciated at $B \approx 0.12 \text{ T}$ in the $3.7 \leq T \leq 4.1 \text{ K}$ isotherms. Since this feature was taken as an indication of the incipient $M(B)$ step related to the SSL phase, we have proceeded to analyze also the second $\partial^2 M / \partial B^2|_T$ derivative of the original $M(B)$ results. The respective curves are collected in Fig. 7c, providing better information to determine the onset of the induced FM

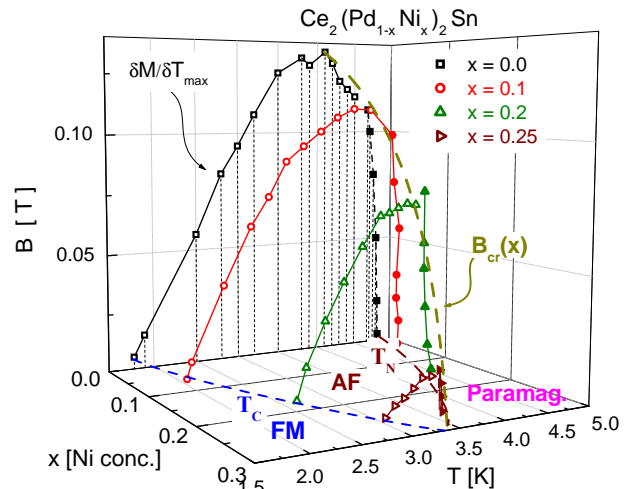


FIG. 8. (Color online) Ni concentration and magnetic field dependent phase diagram in a 3D representation.

phase (main maximum at $B \approx 0.077 \text{ T}$) and the satellite anomaly (see the arrow at $B \approx 0.12 \text{ T}$).

In comparison with the stoichiometric compound, the main maximum has decreased from $B \approx 0.11$ to 0.08 T , whereas the satellite shifted from $B \approx 0.15$ to 0.12 T with a significant reduction in the intensity. Although the B values follow the predictions for a SSL for the appearance of a plateau in the magnetization (at $1/4$ and $1/8$ of the saturated moment [3]), these results from sample $x = 0.1$ are in the limit of our experimental detection. Effectively, in the following concentration studied ($x = 0.2$) no traces of the mentioned anomaly were observed indicating a border line for the SSL formation at $x \simeq 0.1$. Not only the weakening of Ce magnetic moments but also the local disorder due to the difference between Pd and Ni sizes inhibit the Ce-Ce dimers formation with the consequent smearing of the SSL phase.

D. Magnetic phase diagram

The comparison between doping and magnetic field effects is presented in a 3D phase diagram in Fig. 8. There, the field driven transition between intermediate AF and FM-GS phases is drawn according to the temperature of the maximum slope of $M(T)$ (i.e. $\partial M / \partial T|_{max}$) which is in agreement with $C_m(T)$ results. Both phase boundaries join at a critical point, which decreases with Ni content from $T_{cr}(x = 0) = (4.2 \pm 0.3) \text{ K}$ and $B_{cr} = (0.16 \pm 0.02) \text{ T}$ to $T_{cr}(x = 0.25) \approx (3.5 \pm 0.3) \text{ K}$ and $B_{cr} \approx (0.02 \pm 0.005) \text{ T}$, at the edge of the intermediate phase disappearance (i.e. where $B_{cr} \rightarrow 0$). Unfortunately, the tri-critical point where AF, FM and paramagnetic phases join together cannot be reached by doping because it lies beyond the limit of stability of the

Mo₂FeB₂ crystal structure.

The evolution of AF and FM phase boundaries respond to different effects. Starting from high temperature, the decrease of the upper (AF) transition $T_N(x)$ is expected from i) the competition between Kondo effect and RKKY magnetic interactions according to Doniach-Lavagna model [12] acting on the Ce-4f magnetic moments intensity and ii) the local atomic disorder introduced by alloying atoms of different sizes. Both effects weaken the formation of magnetic Ce-dimers on which the SSL builds up. On the contrary the $T_C(x)$ increase is a consequence of the intermediate AF phase weakening like in Ce₂Pd₂Sn under applied magnetic field [8].

The effect of magnetic field is qualitatively similar for each concentration accounting that the range of stability of the AF phase is progressively reduced. Notably, the $\partial M/\partial B|_T$ derivatives of sample $x = 0.25$ still display a weak maximum in a restricted range of field and temperature. This indicates that the critical Ni concentration is not reached yet despite in the $C_m(T)$ cusp of that sample both phase boundaries seem to have converged. Interestingly, the critical temperature T_{Cr} reached by doping at zero field and by magnetic field applied on the stoichiometric compounds are very similar. This confirms the equivalent effect of both parameters on the suppression of the intermediate phase.

IV. CONCLUSIONS

We have seen that Ni doping on Ce₂Pd₂Sn strongly affects the intermediate AF phase of this compound. While the $T_N(x)$ transition decreases, $T_C(x)$ increases following a first order transition line with an end critical point. In fact, at zero field, $T_N(x)$ and $T_C(x)$ converge right above the highest Ni concentration studied ($x = 0.25$). The increase of the FM-GS phase is simply due to the fact that the 2D-AF character weakens respect to the 3D-FM magnetic interactions ones the inter-plan interaction becomes relevant. The progressive weakening of the magnon gap to its disappearance coincides with this behavior.

The SSL phenomenology was hardly recognized from the $M(B)$ dependence only in the 10% doped Ni sample, for higher concentrations (i.e. $x = 0.2$) none of those symptoms have been recognized. Since hybridization effects are only marginal, one concludes that atomic disorder plays an important role inhibiting the SSL phase formation. Magnetic field further weakens the intermediate phase like in the stoichiometric compound, and allows to better define the tri-critical point extrapolated at $T_{cr} \approx 3.4$ K and $x = 0.3$, where $B_{cr} \rightarrow 0$. Unfortunately $x = 0.3$ lies within the structural instability range. Nevertheless, further attempts to get closer to that critical point, and to investigate the Ni-rich side of the phase diagram are in progress.

ACKNOWLEDGMENTS

The author acknowledges L. Amigo and J. Luzuriaga for magnetic measurements. This work was partially supported by PICTP-2007-0812 and SeCyT-UNCuyo 06/C326 projects.

-
- [1] T.R. Kirkpatrick and D. Belitz, Phys. Rev. B **67** 024419 (2003).
 - [2] B.S. Shastry and B. Sutherland; Physica **108B** 1069 (1981).
 - [3] S. Miyahara and K. Ueda; Phys. Rev. Lett. **82** 3701 (1999).
 - [4] M.N. Peron et al., J. Alloys and Comp. 201 (1993) 203.
 - [5] J.G. Sereni, M. Gomez-Berisso, A. Braghta, G. Schmerber and J.P. Kappler, Phys. Rev. B **80** 024428 (2009).
 - [6] M.S. Kim and M.C. Aronson; J. Phys.: Condens Matter **23** (2011) 164204.
 - [7] B.H. Bernhard, B. Coqblin, C. Lacroix Phys. Rev. B **83** 214427 (2011).
 - [8] J.G. Sereni, M. Gomez-Berisso, G. Schmerber, A. Braghta and J.P. Kappler; Phys Rev. B **81** (2010) 184429.
 - [9] Y. Ijiri and F.J. DiSalvo, Jour. Alloys and Compounds **233** 69 (1996)
 - [10] J.G. Sereni, G. Schmerber, A. Braghta, B. Chevalier and J.P. Kappler; ArXiv: cond-mat; 1103.0190v1, 1 March 2011.
 - [11] H.-U. Desgranges and K.D. Schotte, Physics Letters **91A** (1982) 240.
 - [12] S. Doniach, Physica B+C **91** (1977) 231 and C. Lacroix, M. Lavagna and M. Cyrot. J. Phys.,F12 (1982) 745.